Catalysis Science & Technology

Deactivation and regeneration of carbon supported Pt and Ru catalysts in aqueous phase hydrogenation of 2-pentanone

Journal:	*Catalysis Science & Technology*
Manuscript ID	CY-ART-01-2020-000163.R1
Article Type:	Paper
Date Submitted by the Author:	12-Mar-2020
Complete List of Authors:	Huo, Jiajie; Iowa State University, Chemical and Biological Engineering Department; Iowa State University Pham, Hien; U. New Mexico, Chemical & Biological Engineering Cheng, Yan; Iowa State University, Chemical & Biological Engineering Lin, Hsi-Hsin; Iowa State University, Chemical and Biological Engineering Department Roling, Luke; Iowa State University, Department of Chemical & Biological Engineering Datye, Abhaya; University of New Mexico, Department of Chemical and Nuclear Engineering Shanks, Brent; Iowa State University, College of Engineering

ARTICLE

Deactivation and regeneration of carbon supported Pt and Ru catalysts in aqueous phase hydrogenation of 2-pentanone

Received 00th January 20xx,
Accepted 00th January 20xx

DOI: 10.1039/x0xx00000x

Jiajie Huo,[ab] Hien N. Pham,[bc] Yan Cheng,[ab] Hsi-Hsin Lin,[ab] Luke T. Roling,[a] Abhaya K. Datye,[bc] Brent H. Shanks[ab*]

Aqueous phase conversion of biomass-derived molecules requires development of catalysts and operating strategies that create viable operation for extended performance as necessitated for industrial applications. While structural collapse of the support and sintering/leaching of the supported metal particles have been reported in the literature as being primary deactivation mechanism, carbon deposition was found to be the dominate deactivation mode for carbon supported Pt catalysts in aqueous phase 2-pentanone hydrogenation reactions. A mild regeneration method involving air oxidation at 200 °C and H_2 reduction at 180 °C led to full recovery of the catalytic activity. The regeneration method was also successfully applied to Ru catalysts leading to full recovery of activity. The mild regeneration method demonstrated likely has applicability to catalyst regeneration for additional aqueous phase reactions with oxygenated molecules.

Introduction

Aqueous-phase reactions have been explored extensively as biomass conversion to chemicals or fuels commonly is performed in water at high temperatures.[1-3] While active and selective supported metal catalysts are being developed for aqueous phase biomass-related reactions, hydrothermal stability of these materials is one of the key challenges to be solved for scale-up and industrial applications.[4-6] Understanding the underlying deactivation mechanisms is crucial for developing strategies to stabilize the catalysts as well as to regenerate them for recovering activity.[7] Common catalyst supports such as alumina, silica, and zeolites, which are used widely in gas-phase reactions or condensed-phase organic solvent-based reactions, are generally not stable under aqueous-phase reaction conditions as silica and alumina lost more than 70% of surface area when exposed to water at 200 °C for 10 h.[8-10] Additionally, the metal particles on carbon supported monometallic Ru, Pd, Pt, and bimetallic Pt-Re catalysts may undergo deactivation by poisoning, carbon deposition, sintering, leaching, and restructuring separately or concurrently with support collapse/dissolution in various aqueous phase oxidation, reduction, deoxygenation, and hydrogenation at different temperatures ranging from 50°C to 300 °C.[8, 10-21] Due to the harsh hydrothermal reaction conditions, sintering and leaching of the metal particles has commonly been presumed to be the major deactivation mechanism for aqueous-phase reactions.[12, 13, 18-21]

Carbon deposition (coking) is known to be an deactivation mechanism for metal oxide and supported metal materials in gas phase reactions, such as with methane reforming and alkane dehydrogenation.[22, 23] In contrast, there is very limited understanding of deactivation phenomena caused by carbon deposition in aqueous phase biomass conversion catalysts. For example, no regeneration method has been developed to fully recover the catalytic activity from carbon deposition. Also, the nature of carbonaceous species formed on the catalyst are not well understood, partly due to carbon deposit (coke or graphitic carbon) characterization techniques such as in-situ IR and Raman spectroscopy, developed for metal oxide and metal catalysts in high temperature gas phase reactions, being inadequate for aqueous phase reactions. Typical regeneration methods applied to metals supported on metal oxides for removing coke include oxidation and reduction at temperatures higher than 400 °C. Similar regeneration conditions have been applied for regeneration of catalysts used in some aqueous-phase reactions.[20, 21, 24] While carbon supports are generally stable under hydrothermal conditions without any further modifications, they have relatively poor thermal stability compared with metal oxides. Oxidation at high temperature commonly can lead to combustion of the carbon support and typically regeneration such as reduction at 350 °C can result in metal sintering.[25]

Here, we studied the deactivation of carbon supported Pt and Ru catalysts in aqueous-phase oxygenate reduction, where a mild regeneration method involving air oxidation and H_2 reduction at low temperature is shown to result in full recovery of the catalytic activity. These results demonstrate carbon deposition

[a] Department of Chemical and Biological Engineering, Ames, Iowa 50011, United States
[b] Center for Biorenewable Chemicals, Iowa State University, Ames, Iowa 50011, United States
[c] Department of Chemical and Biological Engineering and Center for Microengineered Materials, University of New Mexico, Albuquerque, New Mexico 87131, United States

† Electronic Supplementary Information (ESI) available. See DOI: 10.1039/x0xx00000x

instead of metal particle sintering as a primary deactivation mode.

Experimental

Catalyst synthesis

The carbon black, XC72R (Cabot), was used as received. Incipient wetness impregnation of aqueous H_2PtCl_6 (Sigma-Aldrich) solution was used to synthesize 1%Pt XC72R followed by drying at 80 °C in an oven overnight and reducing in H_2 at 300°C for 2 hr. The synthesis of 1% Pt PANI XC72R (Figure S1) was modified from a reported method.[26] Carbon black XC72R (800 mg) was mixed with aniline (Sigma-Aldrich, 99.5%, 200 mg) in 100 mL of 1M HCl solution and sonicated for 1 h. A 490 mg of $(NH_4)_4S_2O_8$ (Sigma-Aldrich, 98%) was dissolved in 100 mL of 1M HCl solution and added to the mixture of carbon black and aniline dropwise with vigorous stirring at room temperature. The solution was quickly transferred into a water chiller where the temperature was held at 4 °C for 18 h. After polymerization, the PANI coated XC72R was vacuum filtered, washed with water, and dried in an oven at 80 °C for 6 h. An appropriate amount of H_2PtCl_6 was dissolved in water and loaded onto the PANI coated XC72R after drying by incipient wetness impregnation method with 1 wt% Pt loading. The catalyst was dried in an oven at 80 °C overnight and then carbonized at 600 °C for 1 h (ramp rate of 10 °C/min) in a flow of UHP argon, with the catalyst placed in a ceramic boat sitting inside a furnace tube. To compare with 1% Pt PANI XC72R, 1% Pt C XC72R was also prepared with 1 g of XC72R and 0.5 g of glucose in aqueous solution.[19] The glucose amount of 0.5 g was used to yield a similar carbon coating amount as with the PANI coating. After stirring at room temperature to evaporate the water, the slurry was dried in an oven at 80 °C. The same incipient wetness impregnation of H_2PtCl_6 and carbonization at 600 °C for 1 h was used to prepare the catalyst. For the Ru catalyst, $RuCl_3 \cdot xH_2O$ (Sigma-Aldrich, 99.98%) was used to synthesize 1% Ru XC72R and Ru PANI XC72R in the same manner as with the Pt catalysts. 1% Pt AC was purchased from Sigma-Aldrich while 0.5% Ru AC was purchased from Strem and directly used without any treatment.

Hydrothermal treatment (HT)

The hydrothermal treatment of three Pt carbon catalysts (100 mg for each) was performed in a PTFE-lined autoclave together with 30 mL of nanopure water, which was put in a furnace at 170 °C for 48 h in accordance with previous methods.[18, 19] To study prolonged hydrothermal treatment effect on catalyst, 200 mg of Pt AC was treated in the same setup at 200 °C for 50, 100, 150 and 200 h respectively.

Catalyst characterization

BET surface area analysis by nitrogen physisorption was determined using an ASAP 2020 (Micromeritics) at -196 °C with liquid nitrogen after degassing at 150 °C for 5 h. Pore volume was determined at a relative pressure of 0.97. The BJH method was used to evaluate the pore size distribution from the adsorption isotherm. CO pulse chemisorption was performed at 35 °C after reduction in H_2 at 200 °C for 2 hr followed by flushing with UHP argon for 15 min using an ASAP 2920 (Micromeritics) instrument. A stoichiometric factor of 1 was used to calculate metal dispersion.[13] Attenuated total reflectance-Fourier transform infrared spectroscopy (ATR-FTIR) was performed on a Thermo-Scientific Nicolet iS50 FT-IR instrument with a MCT (Mercury Cadmium Telluride) detector. The catalyst powder was placed on an ATR crystal and pressed by the detector. All the spectra were collected at 4 cm^{-1} resolution with 32 scans. Samples were dispersed in ethanol and mounted on holey carbon grids for examination in a JEOL 2010F 200 kV transmission electron microscope. Images were recorded both in bright field (BF) and high angle annular dark field (HAADF) modes. More than 250 Pt particles were counted in the particle size distribution analysis. The surface averaged particle diameter for the Pt particles was calculated using $\sum d^3/\sum d^2$. TGA/DSC-FTIR was performed on a Netzsch STA449 F1 instrument from 35 °C to 500 °C (5°C/min ramp) in 50 ml/min 20% O_2 (UHP grade)/ 80% N_2 (UHP grade). The evolved gas was analysed by an FTIR detector (Bruker Tensor 37) controlled with OPUS software. About 5 mg of fresh or spent 1% Pt AC was first dissolved in 700 µL deuterated DMSO-d_6 (99.5%, Cambridge Isotope Laboratories) and sonicated for 30 min. The catalyst was filtered with a 2 µm filter before H-NMR analysis on a Bruker Avance III 600 NMR instrument. *Ex situ* X-ray Photoelectron Spectroscopy (XPS) was performed on a Kratos/Amicus ESCA3400 instrument with Mg Kα X-rays and analysed with CasaXPS software. The XPS Pt 4f spectra was calibrated with the C1s peak at 284.8 eV.

Reaction testing

Aqueous phase hydrogenation of 2-pentanone was performed in a setup described elsewhere.[27] 40 mg catalyst was loaded in a stainless steel tube (quarter inch O.D.) using quartz wool and silica chips. An HPLC pump (series 1) was used to pump aqueous 2-pentanone (99 %, Sigma-Aldrich) solution (concentration 10 g/L), while a mass flow controller was used to control the flow rate of H_2 gas (20 mL/min, 750 psi). Before each run, the catalyst was reduced in a flow of H_2 (200 mL/min, 750 psi) at 180 °C for 30 min. The temperature was held fixed utilizing a heating tape and PID controller. Samples were collected periodically at the bottom of the condenser and analyzed in GC (Agilent 7890A) equipped with an FID detector and a HP-5 ms column. The condenser was cooled by a water chiller set at 4 °C. 2-pentanol was the only product detected. The molar production of 2-pentanol over the initial 2-pentanone moles was used as the conversion value. The carbon balance was usually above 95%, as shown in the catalytic plots.

Regeneration of catalysts

The in-situ regeneration of the catalysts was performed after stopping the reaction and purging the reactor system with nitrogen gas for 5 min followed by oxidization in 30 mL/min of flowing air at atmosphere pressure at 200 °C for 30 min. After purging with nitrogen gas again for 5 min, the system was switched to hydrogen and the reduction was done at 180 °C with

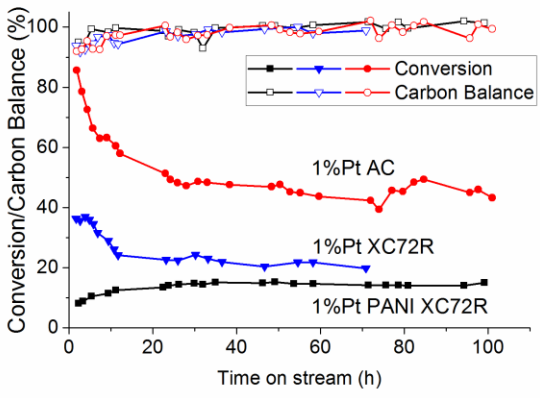

Figure 1. APH of 2-pentanone at 200 °C, 20 mg of catalyst, and 0.08 mL/min 2-pentanone solution with 1% Pt AC, 1% Pt XC72R, and 1% Pt PANI XC72R.

750 psi and 200 mL/min H_2 for 30 min. The reactor temperature was then changed to the desired temperature and the reaction continued with the prescribed conditions. Ex-situ oxidation of the catalyst was also performed to investigate the change in surface area. For comparison, a known amount of commercial 1% Pt AC was placed in a ceramic boat sitting inside a furnace tube with 35 ml/min air at 200 °C for 1, 2, or 3 h.

Results and Discussion

Shown in Figure 1 is the reaction data in which the conversion with 1% Pt AC decreased from 85% to ~50% conversion in the first 30 h and stabilized for the next 70 h. Similarly, 1% Pt XC72R decreased in activity in the first 12 h followed by stability over 60 h time on stream. For 1%Pt PANI XC72R the conversion increased initially followed by a stable but lower activity level compared with the 1% Pt AC and 1% Pt XC72R. This activity was improved by decreasing the PANI loading during synthesis, which is possibly due to higher dispersion of Pt in the thinner, larger pore volume PANI coating (Figure S2).

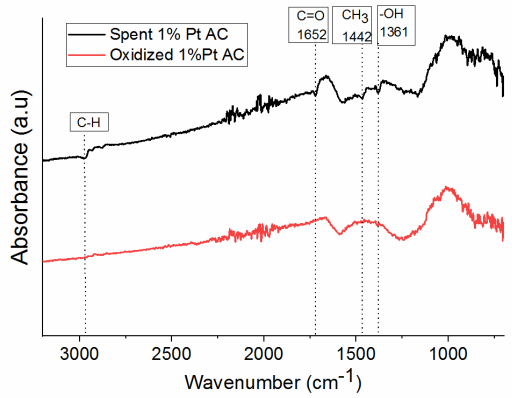

Figure 2. ATR-FTIR spectra of spent 1% Pt AC and the spent 1% Pt AC after oxidization (oxidized 1% Pt AC) in air at 200 °C for 30 min. Fresh 1% Pt AC was used as background and subtracted from both spectra.

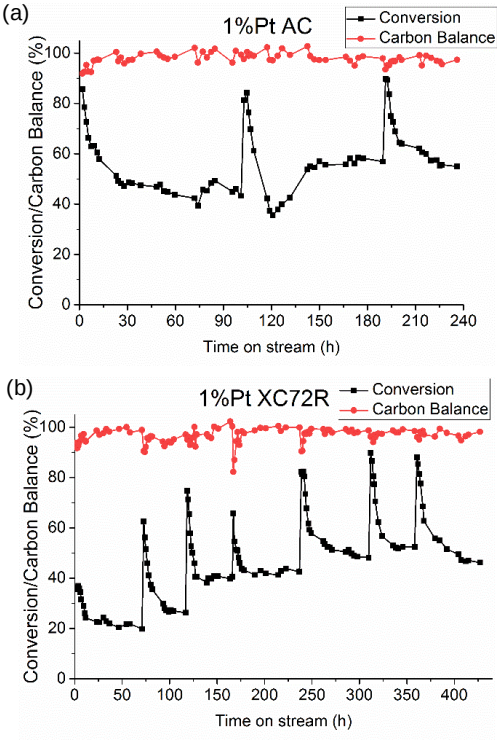

Figure 3. APH of 2-pentanone at 200 °C, 20 mg of catalyst, and 0.08 mL/min 2-pentanone solution on (a) 1% Pt AC and (b) 1% Pt XC72R. In-situ regeneration was consisted of oxidation in air at 200 °C for 30 min and reduction in H_2 at 180 °C for 30 min.

ATR-FTIR spectra (Figure 2) showed that some oxygenated chemical species were deposited on the spent catalyst as evidenced by C=O and –OH functional groups on the spent 1% Pt AC. The presence of these species demonstrated that the carbon deposits were not coke (polyaromatic carbon) species, which are commonly observed in high-temperature gas phase hydrocarbon reactions. Typically, carbon deposits are removed from oxide supported metal catalysts used in gas phase reactions through air or oxygen oxidation at temperature higher than 400 °C. However, high temperature regeneration could damage the carbon support and cause metal particle sintering. As a result, a mild oxidation in air at 200 °C for 30 min was performed on the spent catalyst to remove the oxygenated carbon deposits. The C=O and –OH signals disappeared after the mild oxidation, which confirmed the ability to remove effectively carbonaceous species deposited on the catalyst surface.

After about 100 h on stream, the mild oxidation step followed by reduction in H_2 at 180 °C for 30 min was performed on 1% Pt AC (Figure 3(a)), which resulted in full recovery of the initial catalytic activity. However, the catalyst then quickly deactivated before stabilizing at about 60% conversion. A second regeneration was performed at 190 h on stream again resulting in activity recovery to essentially the initial activity followed by a rapid deactivation and stabilization at about 60% conversion. As shown in Figure 3(b), a similar test sequence was performed with the 1% Pt XC72R catalyst. Using the same regeneration at 75 h, the regenerated catalyst activity was even higher than with the fresh catalyst. Subsequent regenerations showed that the catalyst

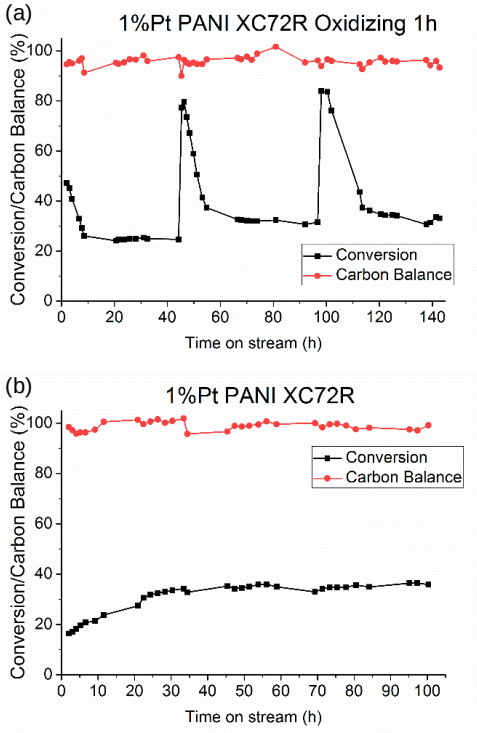

Figure 4. APH of 2-pentanone at 180 °C, 40 mg of catalyst, and 0.08 mL/min 2-pentanone solution; (a) pretreated 1% Pt PANI XC72R and (b) without pretreatment. The catalyst in 4a was first oxidized in air at 200 °C for 1 h and reduced in H_2 for 30 min before reaction.

was regeneratable with peak conversion around 90% and stabilization at about 55% conversion. These results indicated that carbon deposition was the primary deactivation mechanism for the catalyst. It appeared that two different Pt sites existed with one of the Pt sites more prone to carbon deposition. This type of site was deactivated either at the beginning of the reaction or after regeneration. Once these sites were deactivated, the catalytic conversion showed constant stability possibly due to the remaining Pt sites being significantly less prone to carbon deposition.

The mild oxidation/reduction regeneration sequence was used on the fresh 1% Pt PANI XC72R (Figure 4a). This pretreatment resulted in a higher activity at the beginning of the run followed by rapid deactivation and then stabilization. Two subsequent regenerations resulted in similar activity recovery with rapid deactivation and stabilization at around 33% conversion. The control reaction at 180 °C in Figure 4b without pretreatment showed similar activation followed by stable conversion as seen in Figure 1. The higher activity in Figure 4b was a result of different reaction residence time (half as much catalyst was used at 200 °C in Figure 1). The stable conversion in Figure 4a was similar to the control without pretreatment (Figure 4b), suggesting that carbon from the PANI coating could have deposited selectively onto Pt sites that were more prone to deactivation. Similar behaviour has been reported when alumina coating from atomic layer deposition (ALD) preferentially blocked undesired low-coordinated Pt of Pd sites, which were more prone to coke formation.[28-30]

Different adsorption energies on low-coordinated sites versus high-coordinated sites have been reported in computational studies especially for late transition metals such as Co, Ni, Cu, Rh, Pd, Ag, Ir, Pt, and Au, where molecules were found to be more strongly adsorbed on low-coordinated Pt sites (edges and steps) compared with high-coordinated sites (terrace).[29, 31-35] By analogy, it is possible that the carbon deposition-prone Pt was low-coordinated sites, while the stable activity resulted from the remaining high-coordinated sites. If the postulate is correct, the carbonaceous species formed from strongly adsorbed reactants or products on the low-coordinated sites and deactivated these sites, while the high-coordinated sites were responsible for the stable activity after rapid deactivation. Therefore, it is possible that the carbon species generated from PANI during the 1% Pt PANI XC72R carbonization process were similarly strongly adsorbed on these low-coordinated sites. As the highly-coordinated sites were still accessible for reaction, stable catalytic activity with time on stream was observed. When PANI XC72R support was first carbonized followed by impregnation and reduction of Pt, the 1% Pt 600PANI XC72R catalyst behaved like the 1% Pt AC or 1% Pt XC72R, with deactivation at the beginning of reaction followed by stabilization over a long time on stream (Figure S3). Better Pt activity was observed for the PANI coated material compared with glucose coating (Figure S4), which was possibly due to less interaction between the coating and Pt precursor from the less reactive PANI coating structure. The activation at the beginning of reaction on 1% Pt PANI XC72R shown in Figure 4a was likely due to removal of some of the deposited carbonaceous species. When the 1% Pt PANI XC72 was in-situ pretreated with just water, no activation was observed (Figure S5).

The BET surface areas of the three carbon-supported Pt catalysts all had minor increases after 48 h of hydrothermal treatment (Figure 5), which was consistent with the literature.[36] Similar physisorption isotherms (Figure S6) indicated stability of the carbon support structure under hydrothermal conditions. The carbon structure was also maintained during oxidation and prolonged hydrothermal treatment at 200 °C up to 200 h, as evidenced by the minimal change in surface areas and

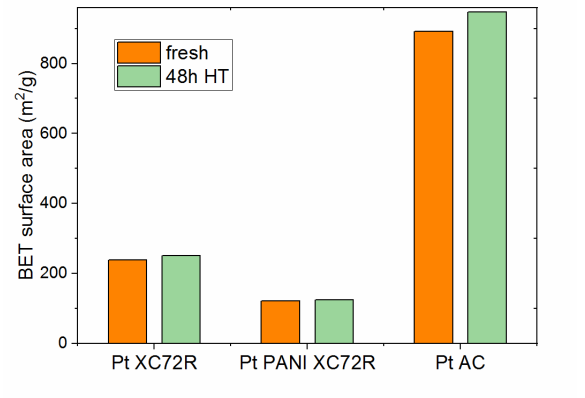

Figure 5. BET surface areas of 1% Pt XC72R, 1% Pt PANI XC72R, and 1% Pt AC before and after 48 h of 170 °C hydrothermal treatment (HT) in water.

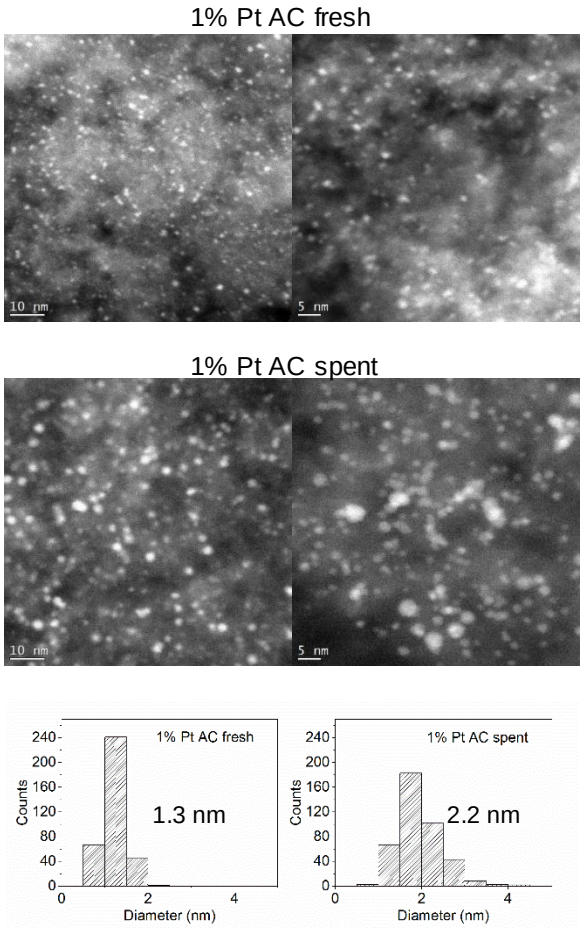

Figure 6. HAADF-STEM images and particle size distribution of fresh and spent 1% Pt AC after 240 h of aqueous phase hydrogenation of 2-pentanone described in Figure 3a. The surface averaged particle size is 1.3 nm for fresh catalyst and 2.2 nm for spent catalyst. The scale bars are 10 (left) and 5 (right) nm, respectively in the TEM images for Figure 6, 7, 8.

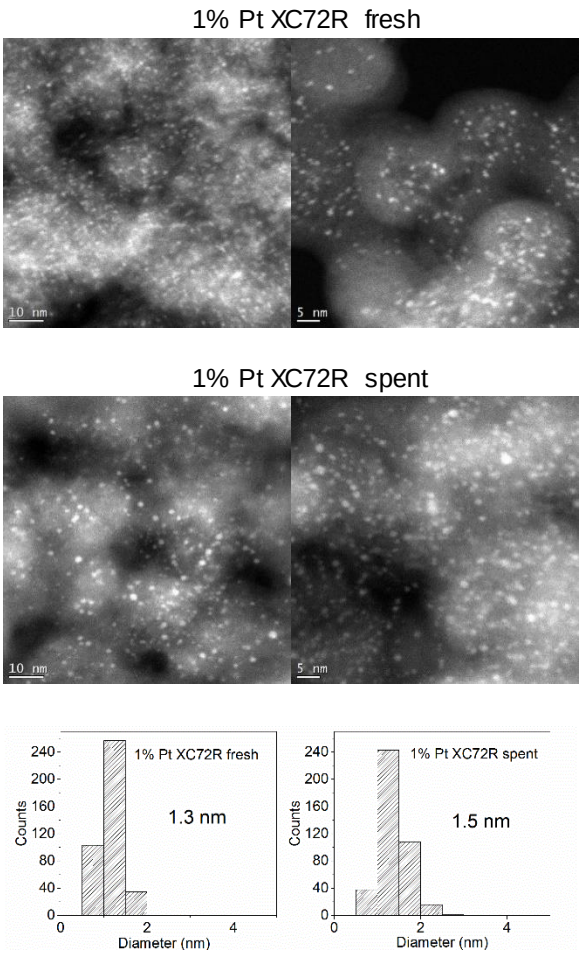

Figure 7. HAADF-STEM images and particle size distribution of fresh and spent 1% Pt XC72R after 450 h of aqueous phase hydrogenation of 2-pentanone described in Figure 3b. The surface averaged particle size is 1.3 nm for fresh catalyst and 1.5 nm for spent catalyst.

physisorption isotherms (Figures S7, S8 and S9). While oxide supports such as silica, alumina and zeolites have poor stability even after shorter hydrothermal treatment, the carbon materials were stable under both hydrothermal and the regeneration conditions in this study.

The gradual activity increase after successive regenerations of 1% Pt XC72R (Figure 3b) suggested that the Pt nanoparticles were initially decorated with some carbon, which was removed by oxidation step during regeneration.[25] When this carbon was gradually removed, the 1% Pt XC72R gave increased activity with a peak conversion of 90% and a stable conversion of 55% by the end of the run. The "decorative" carbon behaved differently than carbonaceous reaction deposits as it impacted both the peak and stable activity whereas the carbonaceous deposits appeared to primarily affect the low-coordinated Pt sites.

HAADF-STEM analysis of the spent 1% Pt AC and 1% Pt XC72R after use in the APH reaction (Figure 3 runs) revealed the Pt particles sintered slightly from an average size of 1.3 nm to 2.3 nm and 1.3 nm to 1.5 nm, respectively (Figures 6 and 7). In contrast, the average Pt particle size remained at 1.6 nm on

Table 1. CO chemisorption data of fresh and hydrothermally treated 1% Pt AC, 1% Pt XC72R, and 1% Pt PANI XC72R in pressurized water at 170 °C for 48 h. HT refers to hydrothermal treatment.

Sample name	Fresh			48 h HT		
	CO uptake/μmol/g	Dispersion/%	Particle size/nm	CO uptake/μmol/g	Dispersion/%	Particle size/nm
Pt AC	22.4	44	2.6	15.7	31	3.7
Pt XC72R	16.7	32	3.5	10.9	21	5.3
Pt PANI XC72R	2.6	5	22.0	5.1	10	11.4

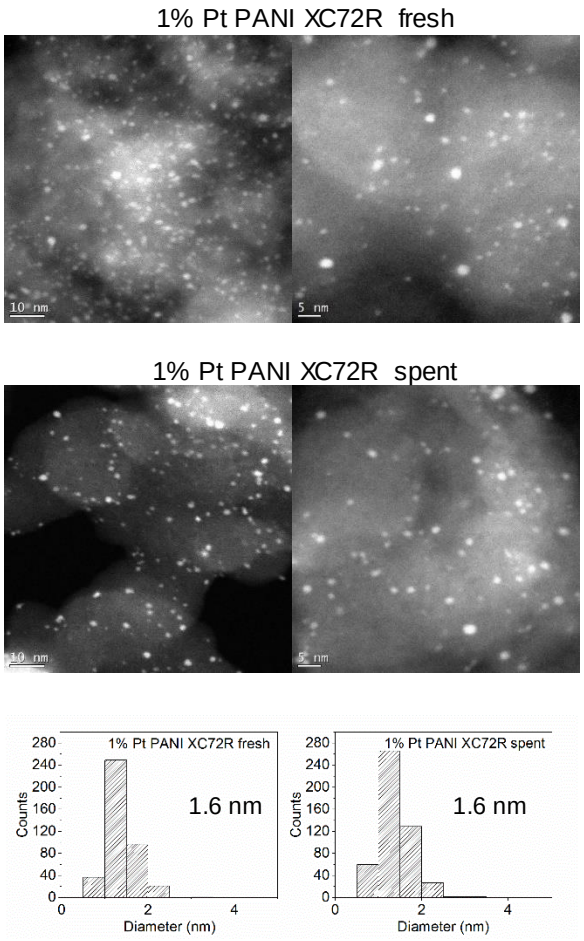

Figure 8. HAADF-STEM images and particle size distribution of fresh and spent 1% Pt PANI XC72R after 100 h of aqueous phase hydrogenation of 2-pentanone described in Figure 1. The surface averaged particle size is 1.6 nm for both fresh and spent catalyst.

PANI XC72R (Figure 8) after reaction, which was consistent with the stable catalytic activity shown in Figures 3 and 4b. The magnitude of the sintering suggested the majority of the activity loss was due to carbonaceous deposition. The stable Pt particles on the 1% PANI XC72R were likely due to the interaction of Pt particles with the coating, which might provide a method to synthesize sinter-resistant supported metal catalysts for these types of reactions. The HAADF-STEM results were consistent with CO chemisorption analysis data after hydrothermal treatment (Table 1), where the Pt particles on Pt AC and Pt XC72R sintered to form larger particles. However, it is worth noting that the particle size estimated from CO chemisorption was nearly twice that from analysis of the HAADF-STEM. This difference was possibly due to decorative carbon covering on the Pt metal particles, which blocked CO chemisorption sites. Also, the dispersion of the 1% Pt AC catalyst decreased further during prolonged hydrothermal treatment at 200 °C for up to 200 h in Table S2. In contrast to the other catalysts, CO chemisorption for the 1% Pt PANI XC72R resulted in particle size significantly larger than seen with HAADF-STEM, which suggested that the particles had significant carbon decorations from PANI coating. This observation was in agreement with the reaction performance, where 1% Pt AC with the highest CO chemisorption value gave the highest activity and 1% Pt PANI XC72 with the lowest CO chemisorption value gave the lowest activity in Figure 1.

Redispersing Pt or Pd nanoparticles in O_2 or Cl_2 gas atmosphere has been reported on zeolite and alumina supported metal catalysts for reforming or oxidation reactions.[37-41] Since the regeneration was performed in air, it was possible that Pt may have been redispersed during the regeneration step. To examine this possibility, the sintered 1% Pt AC catalyst after 200 h of hydrothermal treatment was in-situ oxidized with 10% O_2 in He for 30 min at 200 °C followed by H_2 reduction and CO chemisorption. Table S5 shows that after the 1st oxidation, CO uptake increased somewhat suggesting some possible Pt redispersion. However, the dispersion did not increase further upon successive oxidations and the original dispersion of the fresh 1% Pt AC catalysts could not be fully recovered. After hydrothermal reaction, there was a small amount Pt particle sintering as shown in Figures 6, 7 and Table 1, However, this was not the major deactivation cause as the catalytic activity was fully recovered after regeneration. XPS was performed on the fresh, spent and regenerated 1% Pt AC catalyst to examine the oxidation state of the Pt particles (see Figure S12). Metallic Pt was observed on all of the catalysts, indicating the regeneration condition-oxidation at the temperature of lower than 200 °C did not oxidize the Pt particles. Additionally, in-situ H_2 reduction was always performed before a reaction study and the reaction was conducted in a H_2 atmosphere, Therefore, the XPS results were consistent with the Pt staying in its metallic state during reaction.

While carbon deposition and sintering were both observed with the 1% Pt AC and 1% Pt XC72R catalysts, the rate and the magnitude of the activity loss suggested that carbon deposition during reaction was the primary short term deactivation mechanism. This result was consistent with previous reports that carbon deposition is relatively fast while metal sintering is slow.[39] Additionally, the results with 1% Pt PANI XC72R suggested there was potential to further arrest the metal sintering. To further confirm that carbon species deposition occurred during reaction, TGA-DSC-FTIR was performed on the fresh and spent 1% Pt AC catalyst. TGA-DSC (Figure 9a) showed there was a small decrease in the mass in the beginning period below 120 °C due to physisorbed water removal on the fresh sample. Further temperature increase incurred a slow mass loss until around 400 °C, where a drastic increase and exothermic peak around 400 °C was observed. FTIR spectra on the evolved gas (Figure 9b, 9c) confirmed CO_2 formed during the mass loss and exothermic activity in Figure 9a. The drastic mass loss above 400 °C again confirmed that carbon supports have a low thermal stability. Normal regeneration condition applied on metal oxide materials (oxidation in air) above 400 °C would oxidize the carbon support to CO_2. TGA-DSC of spent 1% Pt AC (Figure 9a) showed different profiles than the fresh catalyst as the major mass loss started around 100 °C with an exothermic peak around 160 °C, which confirmed that oxidation in air at 200 °C during regeneration was able to remove the carbon species deposits. FTIR spectra (Figure 9c) showed three distinct peaks at 1180,

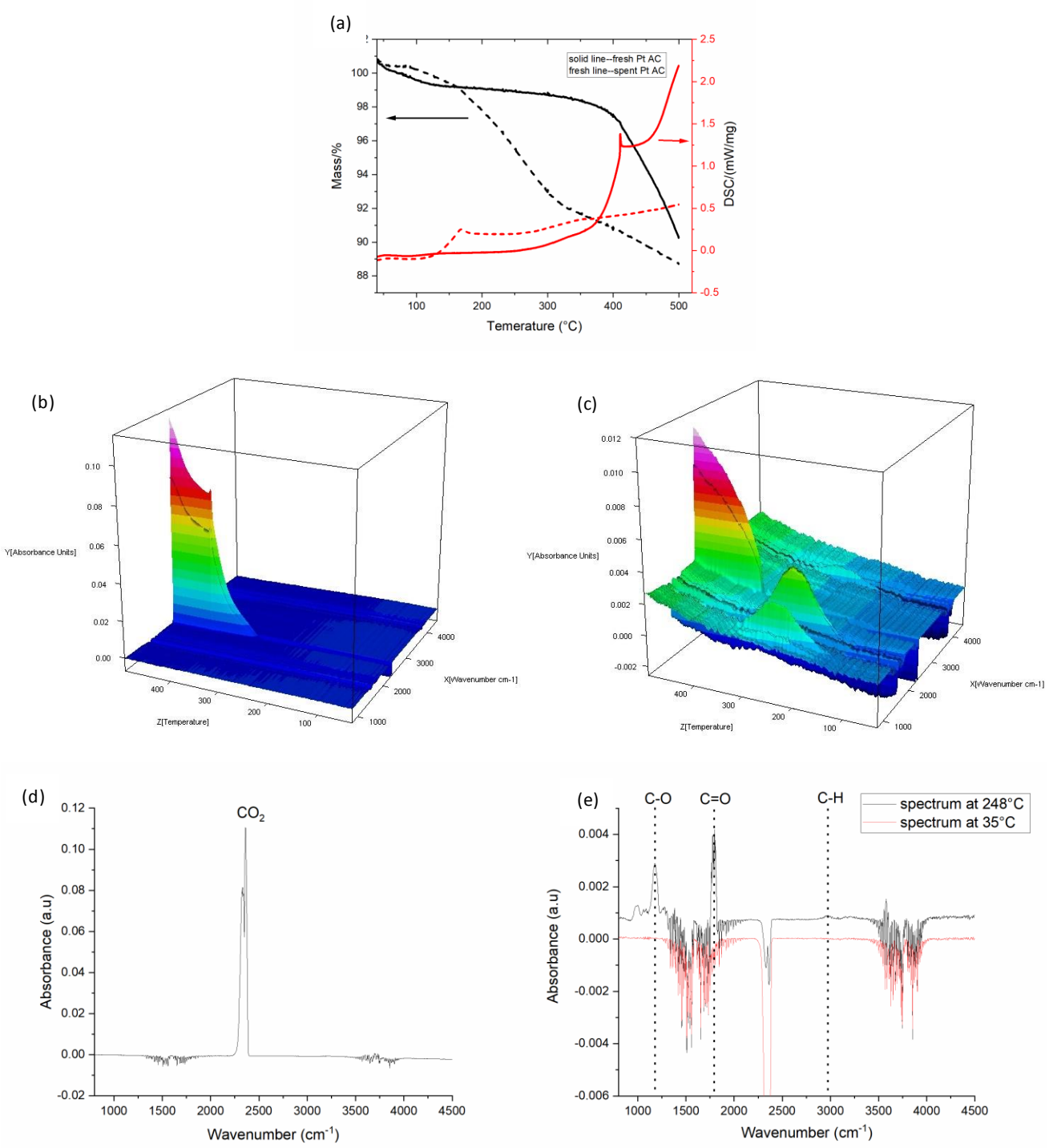

Figure 9. TGA-DSC-FTIR analysis of fresh and spent 1% Pt AC catalyst. TGA-DSC analysis of fresh and spent 1%Pt AC in 20% O2 balanced in N2 (a). 3D FTIR spectra on the envolved gases during TGA on fresh (b) and spent (c) 1% Pt AC. FTIR spectrum on fresh 1% Pt AC at 499 °C (d) and spent 1% Pt AC at 35 °C (red line) and 248 °C (black line) during TGA analysis shown in (a).

1795, 2970 cm^{-1} (Figure 9e) were observed staring around 160 °C, indicating that the carbon deposits on the spent catalyst was decomposed or removed. These carbon fragments from carbon deposits contained C=O, C-O and C-H functional groups. These peaks disappeared around 350 °C and the CO_2 peak became the major peak (Figure 9c), again suggesting carbon support oxidation to CO_2.

As the TGA analysis might have decomposed the carbon deposits on the spent catalyst into smaller carbon fragments, efforts were also made to dissolve the carbon deposits from the spent catalyst in deuterated DMSO with 30 min sonication. The H-NMR spectra in Figure 10 suggested the carbon deposits likely have carboxyl groups and C=C functional groups. However, the exact chemical speciation of the carbon deposits and the

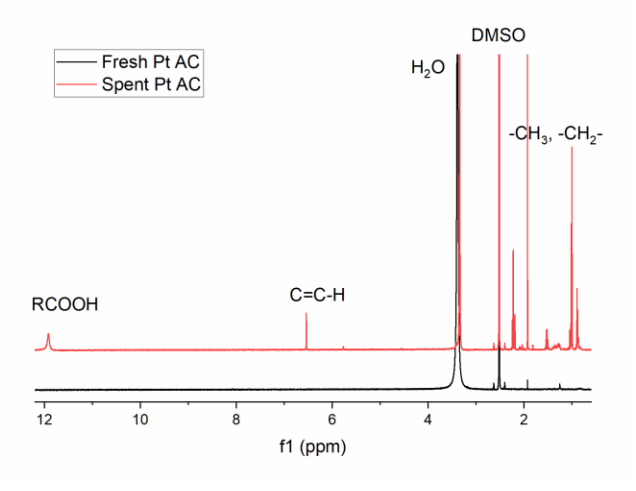

Figure 10. H-NMR spectra of dissolved carbon deposits in DMSO solvent after 30 min sonication of fresh and spent 1% Pt AC.

fundamental deactivation pathway will require future studies. Carboxylate has been reported to deactivate the catalyst during APH of 2-pentanone and levulinic acid.[21] The NMR spectra of the solution after sonicating the spent catalyst as shown here gave direct evidence of the carbon deposits.

As Ru has received attention for 2-pentanone and levulinic acid hydrogenation,[20, 21] Ru catalysts were also synthesized and tested in 2-pentanone hydrogenation. 1% Ru XC72R gave complete conversion at 150 °C, but rapidly deactivated to only about 10% conversion in 70 h (Figure 11a). Using the regeneration procedure given above, the activity was recovered, although the deactivation occurred faster after regeneration. To examine whether regeneration could be achieved with H_2 reduction only, an in-situ H_2 reduction at 180 °C was performed at about 120 h. The conversion only increased from 30% before regeneration to 40% after, which indicated that the oxidation portion of the regeneration was required. A subsequent oxidation/reduction regeneration at about 140 h gave full activity recovery, revealing the requirement for oxidation. Similar behaviour was found when the extended reaction was performed at 100 °C (Figure 11b). Again, the full regeneration procedure resulted in catalyst activity recovery, but a small partial activity recovery was achieved when only H_2 reduction was used for regeneration. For comparison the catalytic performance with regeneration was performed at 50 °C (Figure 11c) as a previous APH study of levulinic acid at 50 °C showed that catalyst activity was partially recovered by only H_2 reduction at 400 °C.[20, 21] It is likely the H_2 reduction used in the prior study did not remove all of the carbon deposits on the catalyst surface. Additionally, the reported Ru particle sintering was likely due to the high temperature regeneration rather than the 50 °C reaction. Regalbuto et al. observed Pd sintering during reduction at 350 °C compared to at 200 °C.[25] Therefore, a suitable regeneration method is needed to just remove carbon deposits without affecting either the metal particles or carbon support.

A 1% Ru PANI XC72R catalyst showed a slower deactivation rate than 1% Ru XC72R at 150 °C (Figure 12). The different behaviour of Ru and Pt on PANI XC72R was likely due to

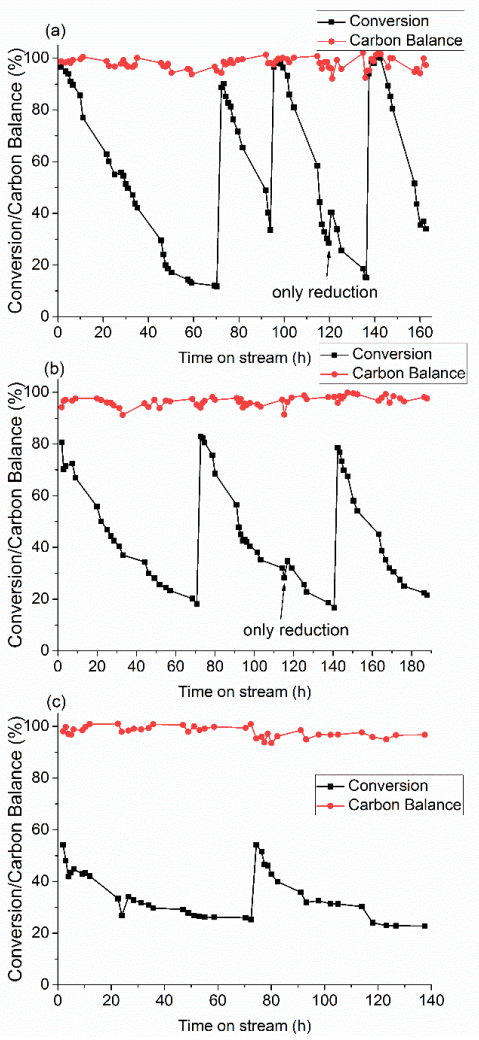

Figure 11. APH of 2-pentanone over 40 mg 1% Ru XC72R at 0.12 mL/min 2-pentanone solution and (a) 150 °C, (b) 100 °C, and (c) 50 °C.

different electrostatic interaction of the cationic Ru precursor compared to the anionic Pt precursor with the PANI coating. Commercial 0.5% Ru AC was used as a benchmark. The fresh catalyst gave less than 2% conversion, but exposure to the full oxidation/reduction regeneration procedure resulted in its activity to 70% conversion that subsequently deactivated quickly

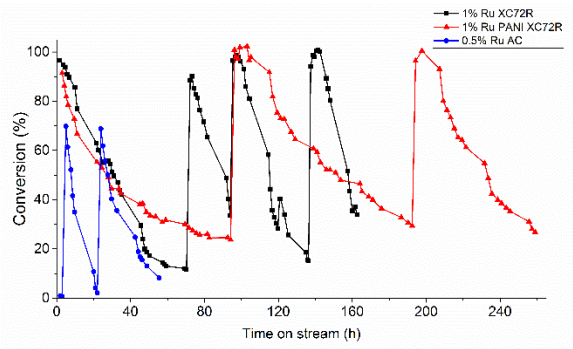

Figure 12. APH of 2-pentanone at 150 °C and 0.12 mL/min 2-pentanone solution over 40 mg 1% Ru XC72R, 0.5% Ru AC, and 1% Ru PANI XC72R.

to 3% in about 20 h. Another regeneration followed the same trend, further showing the importance of in-situ regeneration to recover catalyst activity.

Conclusions

In summary, carbon deposition was identified as the primary deactivation mechanism on carbon supported Pt catalysts. A mild regeneration method that included low temperature air oxidation and H_2 reduction led to full recovery of catalyst activity. The regeneration procedure helped to remove the carbon deposits and gave some minor redispersion of the Pt nanoparticles. Utilizing a nitrogen-containing carbon coating (PANI XC72R) diminished the initial activity of the Pt but may have stabilized the Pt particles against sintering under aqueous phase reaction conditions. TGA-DSC-FTIR and NMR analysis confirmed carbon species deposition from the reaction. The same mild regeneration procedure was able to recover effectively the activity of Ru catalysts. Therefore, the mild regeneration method appeared to be a preferred strategy for reactivating catalysts in aqueous phase reactions of oxygenated compounds rather than the higher temperature regeneration more commonly used for catalysts deactivated in gas phase reactions.

Conflicts of interest

There are no conflicts to declare.

Acknowledgement

This work is supported by the Center for Biorenewable Chemicals funded by NSF grant EEC-0813570. We would like to thank Dr. Le Xin for the discussion about using PANI coating, Zhanyi Yao for his help in experiment, Dr. Brett Boote for his help with TGA-DSC-FTIR analysis, Dr. Dapeng Jing for his help with XPS analysis, Professor Andrew Hillier, Dr. Russell Mahmood, and Dr. Zhiqi Yao for their help with ATR-FTIR analysis. We also thank Professor Jean-Philippe Tessonnier for helpful discussions.

References

1. D. M. Alonso, J. Q. Bond and J. A. Dumesic, *Green Chem.*, 2010, **12**, 1493-1513.
2. J. S. Luterbacher, D. M. Alonso and J. A. Dumesic, *Green Chem.*, 2014, **16**, 4816-4838.
3. G. W. Huber and J. A. Dumesic, *Catal. Today*, 2006, **111**, 119-132.
4. H. Xiong, H. N. Pham and A. K. Datye, *Green Chem.*, 2014, **16**, 4627-4643.
5. J.-P. Lange, *Angew. Chem. Int. Ed.*, 2015, **54**, 13186-13197.
6. T. J. Schwartz, B. J. O'Neill, B. H. Shanks and J. A. Dumesic, *ACS Catal.*, 2014, **4**, 2060-2069.
7. S. L. Scott, *ACS Catal.*, 2018, **8**, 8597-8599.
8. H. N. Pham, A. E. Anderson, R. L. Johnson, K. Schmidt-Rohr and A. K. Datye, *Angew. Chem. Int. Ed.*, 2012, **51**, 13163-13167.
9. D. W. Gardner, J. Huo, T. C. Hoff, R. L. Johnson, B. H. Shanks and J.-P. Tessonnier, *ACS Catal.*, 2015, **5**, 4418-4422.
10. J. Z. Duan, Y. T. Kim, H. Lou and G. W. Huber, *Catal. Today*, 2014, **234**, 66-74.
11. J. H. Xie, P. Duan, N. Kaylor, K. H. Yin, B. Huang, K. Schmidt-Rohr and R. J. Davis, *ACS Catal.*, 2017, **7**, 6745-6756.
12. H. N. Pham, A. E. Anderson, R. L. Johnson, T. J. Schwartz, B. J. O'Neill, P. Duan, K. Schmidt-Rohr, J. A. Dumesic and A. K. Datye, *ACS Catal.*, 2015, **5**, 4546-4555.
13. D. R. Vardon, B. K. Sharma, H. Jaramillo, D. Kim, J. K. Choe, P. N. Ciesielski and T. J. Strathmann, *Green Chem.*, 2014, **16**, 1507-1520.
14. A. S. Piskun, J. E. de Haan, E. Wilbers, H. H. V. de Bovenkamp, Z. Tang and H. J. Heeres, *ACS Sustainable Chem. Eng.*, 2016, **4**, 2939-2950.
15. T. J. Schwartz, Z. J. Brentzel and J. A. Dumesic, *Catal. Lett.*, 2015, **145**, 15-22.
16. E. P. Maris, W. C. Ketchie, V. Oleshko and R. J. Davis, *J. Phys. Chem. B*, 2006, **110**, 7869-7876.
17. J. H. Xie, D. D. Falcone and R. J. Davis, *J. Catal.*, 2015, **332**, 38-50.
18. J. J. Huo, P. Duan, H. N. Pham, Y. J. Chan, A. K. Datye, K. Schmidt-Rohr and B. H. Shanks, *Catal. Sci. Technol.*, 2018, **8**, 3548-3561.
19. J. Huo, R. L. Johnson, P. Duan, H. N. Pham, D. Mendivelso-Perez, E. A. Smith, A. K. Datye, K. Schmidt-Rohr and B. H. Shanks, *Catal. Sci. Technol.*, 2018, **8**, 1151-1160.
20. O. A. Abdelrahman, A. Heyden and J. Q. Bond, *ACS Catal.*, 2014, **4**, 1171-1181.
21. O. A. Abdelrahman, H. Y. Luo, A. Heyden, Y. Roman-Leshkov and J. Q. Bond, *J. Catal.*, 2015, **329**, 10-21.
22. H. N. Pham, J. Sattler, B. M. Weckhuysen and A. K. Datye, *ACS Catal.*, 2016, **6**, 2257-2264.
23. D. L. Trimm, *Catal. Today*, 1999, **49**, 3-10.
24. J. A. Lopez-Ruiz and R. J. Davis, *Green Chem.*, 2014, **16**, 683-694.
25. J. M. M. Tengco, Y. K. Lugo-Jose, J. R. Monnier and J. R. Regalbuto, *Catal. Today*, 2015, **246**, 9-14.
26. L. Guo, W. J. Jiang, Y. Zhang, J. S. Hu, Z. D. Wei and L. J. Wan, *ACS Catal.*, 2015, **5**, 2903-2909.
27. B. J. O'Neill, D. H. K. Jackson, A. J. Crisci, C. A. Farberow, F. Shi, A. C. Alba-Rubio, J. Lu, P. J. Dietrich, X. Gu, C. L. Marshall, P. C. Stair, J. W. Elam, J. T. Miller, F. H. Ribeiro, P. M. Voyles, J. Greeley, M. Mavrikakis, S. L. Scott, T. F. Kuech and J. A. Dumesic, *Angew. Chem. Int. Ed.*, 2013, **52**, 13808-13812.
28. J. L. Lu, B. S. Fu, M. C. Kung, G. M. Xiao, J. W. Elam, H. H. Kung and P. C. Stair, *Science*, 2012, **335**, 1205-1208.
29. G. W. Peng, D. Gerceker, M. Kumbhalkar, J. A. Dumesic and M. Mavrikakis, *Catal. Sci. Technol.*, 2018, **8**, 2159-2174.
30. H. Feng, J. L. Lu, P. C. Stair and J. W. Elam, *Catal. Lett.*, 2011, **141**, 512-517.
31. A. A. Peterson, L. C. Grabow, T. P. Brennan, B. G. Shong, C. C. Ooi, D. M. Wu, C. W. Li, A. Kushwaha, A. J. Medford,

F. Mbuga, L. Li and J. K. Norskov, *Top. Catal.*, 2012, **55**, 1276-1282.
32. X. F. Ma and H. L. Xin, *Phys. Rev. Lett.* 2017, **118**.
33. F. Calle-Vallejo, J. I. Martinez, J. M. Garcia-Lastra, P. Sautet and D. Loffreda, *Angew. Chem. Int. Ed.*, 2014, **53**, 8316-8319.
34. L. T. Roling and F. Abild-Pedersen, *ChemCatChem*, 2018, **10**, 1643-1650.
35. R. M. Watwe, R. D. Cortright, J. K. Norskov and J. A. Dumesic, *J. Phys. Chem. B*, 2000, **104**, 2299-2310.
36. A. H. Van Pelt, O. A. Simakova, S. M. Schimming, J. L. Ewbank, G. S. Foo, E. A. Pidko, E. J. M. Hensen and C. Sievers, *Carbon*, 2014, **77**, 143-154.
37. C. H. Bartholomew, *Studies in surface science and catalysis 1997*, 1997, **111**, 585-592.
38. L. K. Ono, B. Yuan, H. Heinrich and B. Roldan Cuenya, *J. Phys. Chem.C*, 2010, **114**, 22119-22133.
39. M. D. Argyle and C. H. Bartholomew, *Catalysts*, 2015, **5**, 145-269.
40. E. J. Peterson, A. T. Delariva, S. Lin, R. S. Johnson, H. Guo, J. T. Miller, J. H. Kwak, C. H. F. Peden, B. Kiefer, L. F. Allard, F. H. Ribeiro and A. K. Datye, *Nat. Commun.*, 2014, **5**.
41. D. L. Trimm, *Appl. Catal. A*, 2001, **212**, 153-160.

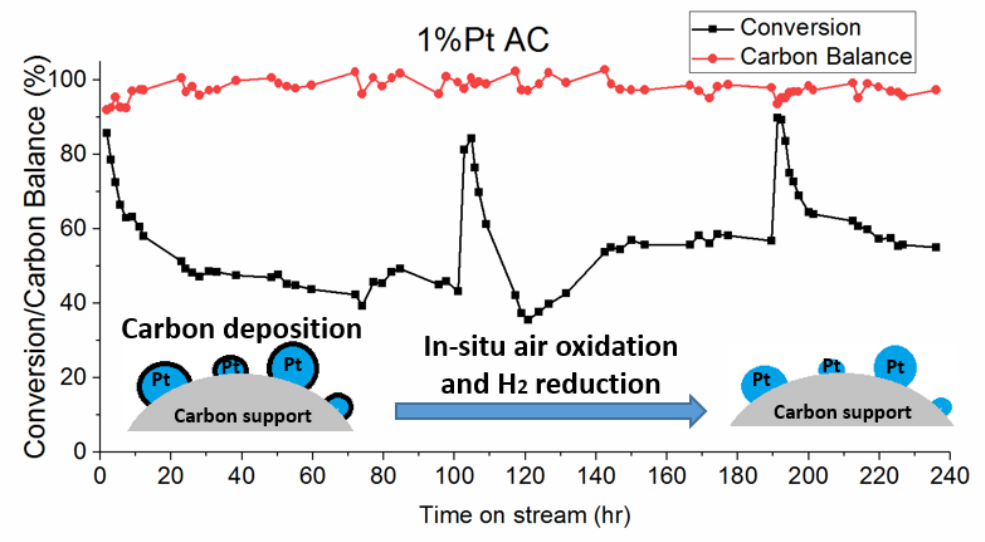

134x73mm (150 x 150 DPI)